5. Formation and Evolution of "Laser-Bullets"- Massive Plasma Blocks with Strong Magnetic Fields

Laser-plasma interaction for moderate intensities of laser radiation (10^{13} - 10^{15} W/cm^2) showed filamentation and formation of jets the diameter of which is substantially smaller than the spot diameter of the incident laser beam [1-4]. Apart from the lateral effects, a very complex temporal stochastic pulsation with a period of about 10 to 50 ps was reported in [5-7]. In a numerical hydrodynamic study [8] it has also been shown that generation of fast moving plasma blocks with velocities beyond 10^8 cm/s is possible due to ponderomotive force in a plasma layer near the critical density. To investigate the processes of channeling and filamentation and, in particular, to measure the time–resolved density distribution in filaments or the strength of self-generated magnetic fields in plasma channels during laser beam propagation, is a rather difficult experimental task. The generation of spontaneous magnetic fields in laser-produced plasmas have been extensively investigated for moderate incident intensities of laser radiation [10-16] and with a development of compact terrawatt lasers also for high laser beam intensities ($I > 10^{18}$ W/cm^2) [17-19]. The first experimental observations of self-generated magnetic fields in laser plasma were explained in terms of a thermoelectric source [10] that originates in a hot collisional plasma when the gradient of the electron temperature ∇T_e is not collinear with the electron density gradient ∇N_e. The spontaneous magnetic field has a toroidal structure, which results from the current loop produced by the ejected hot electrons. These thermoelectrically generated magnetic fields have been seen also at interaction of ultraintense short laser pulses with preionized plasma targets and solid targets [17]. However, for the plasma targets close to the laser axis very high „dc“ magnetic field with opposite orientation was observed. Possible explanation of this laser-driven magnetic field, is its generation due to a strong quasi-steady electron current in a low density plasma

channel [20-22].

In this chapter the first interferometric observations of the dynamics of laser bullets – accelerated thick plasma blocks, generated in air during the interaction of a picosecond laser pulse with an Al-target at irradiances of 10^{14} W/cm^2 will be presented. Futhermore we report about periodical (10-40 ps) self-channeling of laser beam in narrow plasma channels in front of the surface of strong shock waves. High density blocks of plasma move with velocities of about (2 – 4.5) x 10^8 cm/s towards to the laser beam and keep a stable configuration in space and time during the laser pulse. The effect is strongly resonant, the accelerated plasma blocks appear only when the laser pulse energy exceeds 60 mJ (for the pulse duration of 100 ps and the beam wavelength λ =1064 nm). The interaction results then in a strong increasing of the ponderomotive force and in a growth the associated nonlinear phenomena. For Faraday- rotation and interferometric measurements of spatial profiles of the self-generated magnetic fields in all the investigated plasma objects a second-harmonic probe beam was used. The characteristic structure of the measured magnetic fields being "frozen" in moving plasma blocks indicates that the generation of dc magnetic fields occurs due to resonance absorption of laser light.

5.1. Dynamics of "Laser-Bullets"

1. Experimental

An intense horizontally polarized IR pulse (100 mJ, 100 ps, 1064 nm) from Nd:YAG laser was focused by 25 cm focal length lens to the maximum intensity of $8x10^{13}$ W/cm^2 . The laser beam was incident normal on the planar Al target in air. The target was placed in one arm of Michelson interferometer. The probing laser beam at the second harmonic (λ = 532 nm) was optically delayed from – 2 ns to 10 ns with respect to the ignition beam . Imaging of the target and of the focal region of the laser pulse with the resolution of 1 μm were achieved by means of a long-distance microscope Questar 100 placed at a

working distance of 10 cm. A 10nm interference filter centered at λ = 532 nm was used to reduce the light emitted by the laser-produced plasmas. The output images were digitized to 8-bit depth by a CCD camera with a 512x512 pixel frame. The distributions of interference phase were determined by using a special computer code. This arrangement, but using one mirror only, was exploited also for recording plasma shadowgramms. With the Nd:YAG laser pulse of 100 ps FWHM this laser diagnostics gives a „snapshot“ of the density evolution in a laser-produced plasma. In this fashion the refractive index distributions were obtained within the self-focused plasma channel and in the accelerated thick plasma blocks.

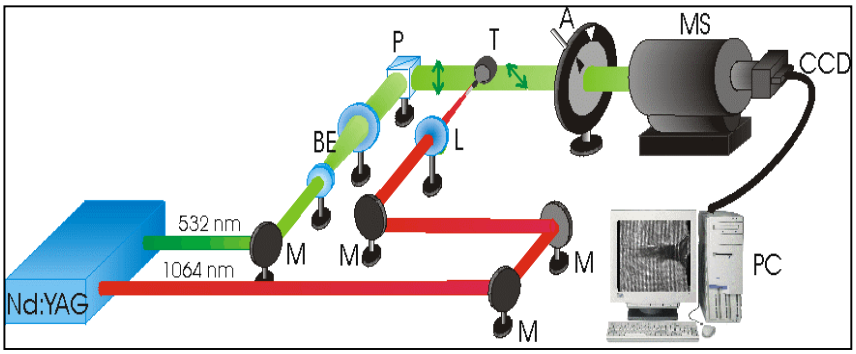

Fig. 1. Experimental setup for detecting the rotation of polarization. Nd:YAG – laser system, M –mirrors, BE – beam expander system, T – target, L – lens, P – polarizer, A – analizer, MS – long-distance microscope, CCD – CCD-camera, PC- automatic image processing.

For studies of the spontaneous magnetic fields the probing beam at λ = 532 nm passed a variable optical delay was vertically polarized by means of the polarizer (P). The experimental setup for Faraday-rotation measurements using a probing beam is shown in Fig. 1. The polarization of the probe beam having passed the plasma was analyzed by using the crossed polarizer (A).The focal spot region was imaged by the long-distance microscope (MS) on the CCD-matrix with the same spatial resolution as at interferometric measurements. Images were recorded for different delay times of the probe beam relative to the peak of the main pulse. The analyzer was rotated with the step of Δφ = 1° for

both negative and positive rotation angles, starting from the fully crossed position of the polarizers. For each rotation angle more than 10 polarogramms were recorded, with a good shot-to-shot reproducibility. In order to examine the influence of depolarization of the probing beam and to reduce errors at reconstructing the rotation angle, the measurements were carried out for two incident angles of the probing beam : $\phi = 0$ and $\phi = \pi/4$, where ϕ is the angle between the wave vector **k** of a probe electromagnetic wave and the magnetic-field induction vector **B** in a magnetoactive plasma. For "quasilongitudinal" propagation of the electromagnetic wave ($\phi = 0$) due to the Faraday effect we obtain the expression for rotation angle Θ in following form [23]

$$\Theta = -2.77 \cdot 10^{-17} \lambda^2 \int_0^L B_{II} N_e dl \quad (rad) \qquad (1)$$

where λ is the probe beam wavelength in cm, N_e is the electron density in cm^{-3}, B_{II} is the component of magnetic field induction **B** along the vector **k** in Gauss, L is the probe-beam path.

Inhomogeneities of the electron density, velocity and temperature in laser-produced plasmas can lead to an appreciable growth of changes in the polarization state of the probing wave. In case of the Cotton-Mouton effect the phase shift for depolarization of the probing electromagnetic wave can be written in the following form

$$\Theta = 2.47 \cdot 10^{-21} \lambda^3 \int_0^L B^2 N_e \, dl \quad (rad) \qquad (2)$$

Since the rotation mechanisms are additive, the resultant rotation of the polarization plane of probing beam includes both components. But contribution to the rotation angle due to the Cotton-Mouton effect is two-three orders of magnitude smaller, than that due to Faraday effect.

For "quasitransverse" propagation of the electromagnetic probe wave the phase shift is given by [23]

$$\Delta\varphi = 2\sin(4\psi)\left[\ \frac{2\pi}{\lambda}\int_0^L (n_L - n_0)dl\ \right]^2 \qquad (3)$$

and the change of the polarization ellipticity by

$$\Delta k = \sin(2\psi)\frac{2\pi}{\lambda}\int_0^L (n_L - n_0)dl \qquad (4)$$

where (n_L - n_0) is the change of the refraction index during the probe beam propagation through the magnetoactive medium along the path L, ψ is the angle between the polarization plane of the probe beam and the direction of plasma inhomogeneity (temperature and pressure gradients). By choosing $\psi = \pi/4$, so long as the density and temperature gradients are oriented along and perpendicular to the target surface, we eliminate the component connected with the rotation of the polarization plane $\Delta\varphi$ and with the increase of the depolarization signal Δk. This procedure allowed us to determine correctly the influence of depolarization on the magnitude of rotation angle due to Faraday effect.

Interferometric and shadowgraphic measurements of the laser-produced plasma were carried out in parallel with polarimetric measurements. By taking into account the axial symmetry of the investigated plasma, it was possible to reconstruct the distribution of the magnetic induction vector B(r,z) for different delay times relative to the laser pulse

2. Stochastic Pulsation and Formation of "Laser Bullets".

All experiments were carried out in air. A significant feature of our experimental set-up is the amplified spontaneous emission (ASE) arising in long pre-pulse (ns-range). The value of the contrast of laser radiation in the main peak to the pedestal radiation is 150 only , so the intensity in the pre-pulse was about 5 x10^{11} W/cm^2, which is well above the generally accepted long pulse threshold intensity for plasma generation in air [24]. By focusing the heating

laser beam to the spot size of 30 μm in front of the target, it was possible to form a low density plasma before the main pulse with I = $8x10^{13}$ W/cm^2 reached this region. It is evident from Fig.2, in which the time history of the propagation of a horizontally polarized laser pulse (energy100 mJ, pulse duration 100 ps and wave-length λ = 1064 nm) is shown. The times indicated at each image in Fig.1 correspond to the time delay between the probe pulse and that of the heating beam. The shadowgramms in Fig.2a clearly show a shock wave front with a steep density gradient, which is formed ~ 2 ns before the pulse center of heating beam reaches this point. The electron density in front of the shock wave determined from interferogramms is of the order of 10^{20} cm^{-3} , the front width being of about 5 μm. Strong absorption of laser radiation in this thin plasma layer is witnessed by a characteristic plasma emission at the second harmonic of laser frequency. In the shadowgramm recorded at t = -700 ps (Fig. 2b) the $2\omega_0$ emission in the form of a concave disk with the diameter of 50 μm is clearly visible. This is the region where the incident laser frequency ω_0 equals the plasma frequency ω_p and the conditions for resonant absorption are fulfilled. For p-polarized laser heating pulse $\omega_p = \omega_0 \cos\theta$. By taking $\cos\theta = 0.3$ from Fig. 1b, we obtain N_e = 1.2 $x10^{20}$ cm^{-3} , which is in good agreement with the interferometric plasma density measurements. When the leading part of the heating pulse penetrates the plasma with such a density gradient, a narrow filament about 5 μm in diameter and 200 –300 μm long accompanied with strong shock waves appears (Fig. 2c) . One shock wave (2) propagates with the velocity of $6x10^7$ cm/s towards the target (its front 2 is clearly visible in Fig.1c), and another one (1) in the opposite direction, towards the heating laser beam, with V = $2.25x10^8$ cm/s. The filament formation at longer delay times is shown in Fig.2d, 2e, 2f. It should be noted, that the filaments are formed in front of the shock waves displaced one with respect to another by Δl~30-50 μm. When taking into account that filaments are formed during the the heating pulse and

each shadowgramm gives a "frozen" 100-ps snap shot of the interaction , then the average pulsating time of filaments can be calculated as $t = \Delta l/V = 13\text{-}22$ ps.

Besides the filamentation, for later delay times we have observed accelerated massive plasma blocks (fragments) moving towards the heating beam. These plasma fragments retain the concavo-convex configuration of the resonance absorption layer. In some cases, the boundary in the abrupt pulled off fragments is not smooth its outline copying exactly the same outline boundary in the remaining plasma body.

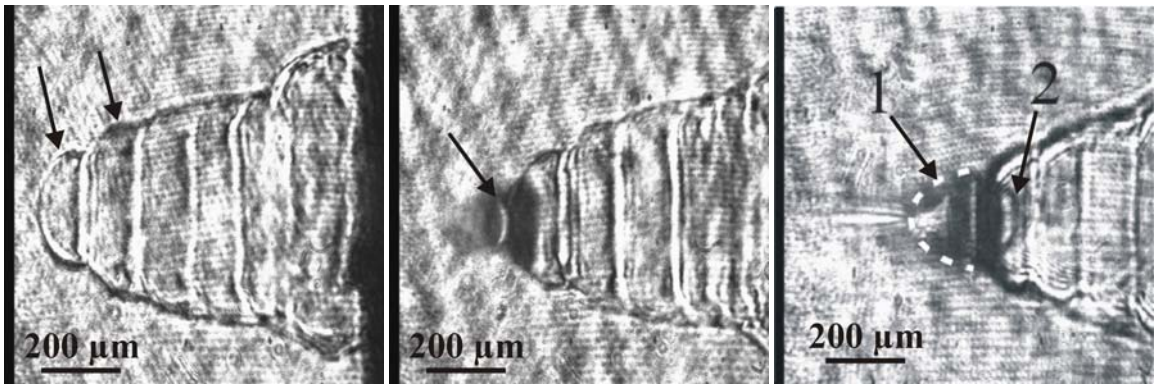

(a) - 2 ns (b) - 700 ps (c) - 120 ps

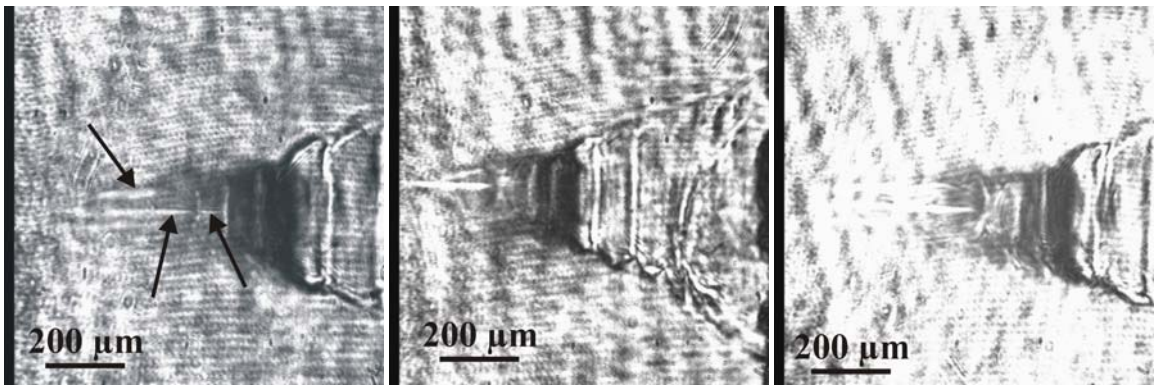

(d) - 120 ps (e) - 60 ps (f) -30 ps

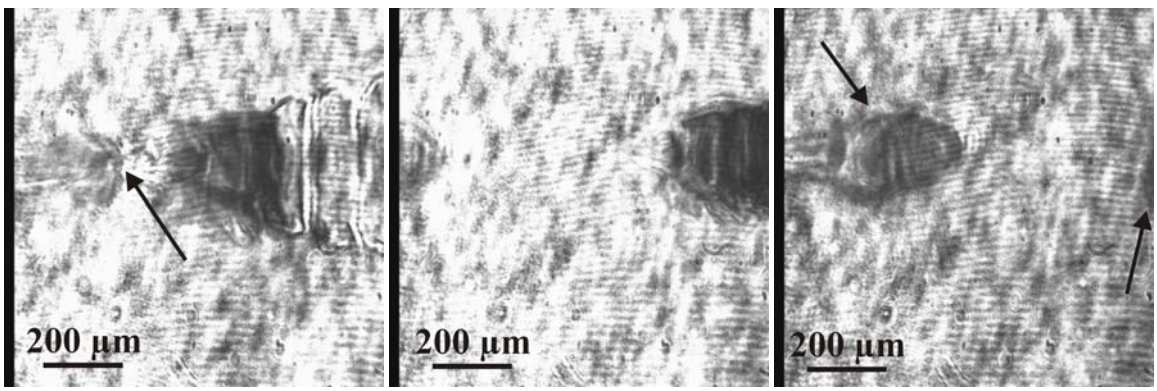

(g) +30 ps (h) +60 ps (i) +60 ps

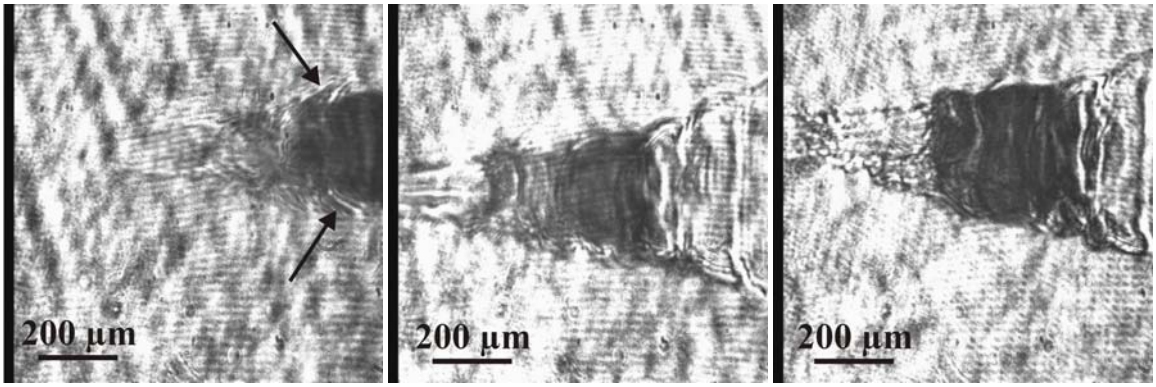

(j) +60 ps (k) +200 ps (l) + 1000 ps

Fig. 2. Schadowgrams showing the time history of laser beam interaction with the preformed plasmas for propagation of 100 mJ laser pulse (from left) in air near the Al-target (right). Delay times between the probe pulse at 532 nm and heating beam at 1064 nm are indicated below each image (a) The arrows show the narrow shock wave fronts created in the pre-pulse stadium.(b) Self-emission at 2ω marked by arrow assigns a resonance absorption surface. (c) With 1 and 2 marked arrows show an oppositely directed shock wave fronts. Self-focusing of laser beam to filaments of 5 µm diameter is evident in front of shock wave (left). (d) Filament formations in front of shock waves are shown by arrows.(g) Arrows indicate the moment of plasma block disruption and moving been left plasma fragment. (j) Mach whiskers are shown by arrows.

Figure 2g illustrates the moment of disruption of a plasma fragment from the plasma body, while the moving off plasma blocks – "laser bullets" - are well seen in Fig.2h and 2i. The shadowgramms in Fig. 2j, 2k, 2l show examples of the plasma targets after the blowing off the "light bullets". Close to the point of disruption a shock wave structure with Mach whiskers typical for a hydrodynamic blow was observed (in Fig.2j). These Mach whiskers are marked by arrows). For later delay times (t = 400 –1000 ps) the shock wave fronts extinguish again.

From many series of such shadowgramms (some more examples are presented in Fig.3) it was possible to estimate the average velocity and the acceleration of the moving plasma blocks(3.3 ± 1.3)x10^6 m/s and (7 ± 3)x10^{16} m/s^2 , respectively). . As all the data are time integrated over the 100-psec laser

pulses used, the maximum instantaneous velocity and acceleration values may be even higher.

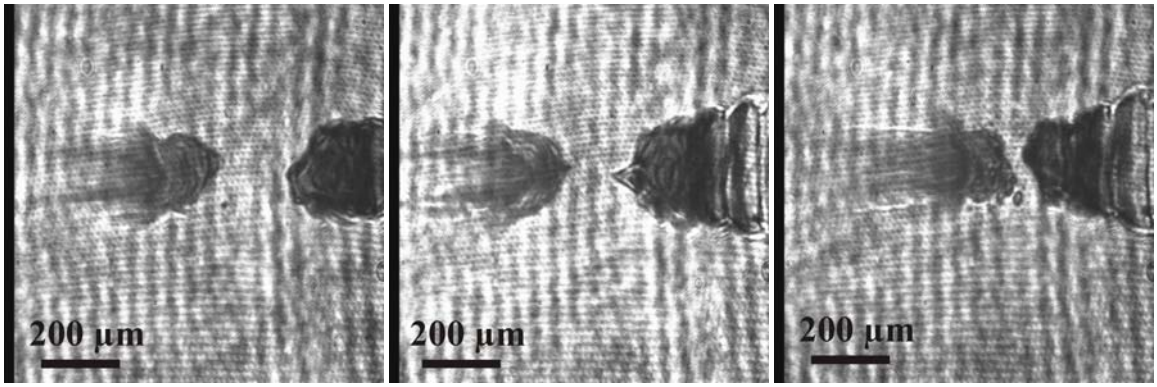

(a) (b) (c)

Fig. 3. "Laser bullets" for delay time t = 60 ps.

Direct measurement of density profile distributions within the self-focused plasma channel and accelerated thick plasma blocks have been made with high temporal and spatial resolution by means of interferomety. Figures 4, 5, and 6 feature the radial electron density profiles for a delay times t = 0 ps, 30 ps and 130 ps. A sharp electron density front propagaiting toward the incident laser wave is evident at t = 0 ps and t = 30 ps. The mean electron densities arrive values on order of $(1 – 2.5)x\ 10^{20}$ cm^{-3}. The filaments have a typical diameters of 8 – 15 μm. A rippling of the density and cavitons production by the nonlinear force can also be seen from interferogramms.

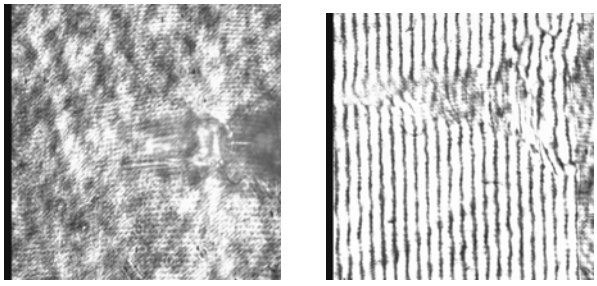

(a) (b)

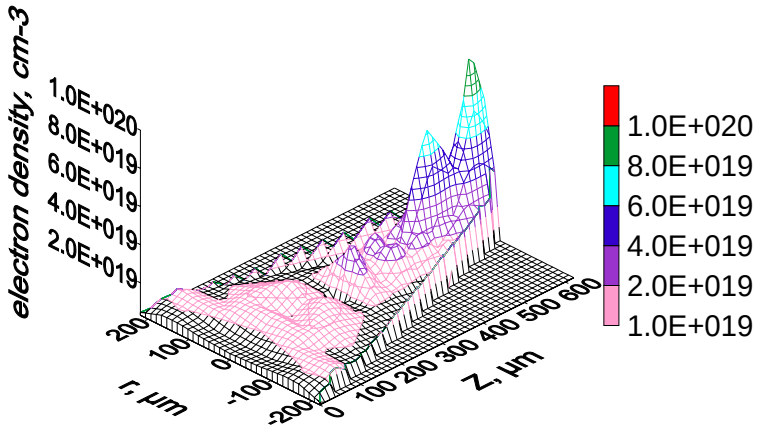

Figure 4. An absorption image (a), interferogram and electron density distribution for delay time t = 0 ps. A moment of disconnetion of plasma block is fixed in (a) and (b).

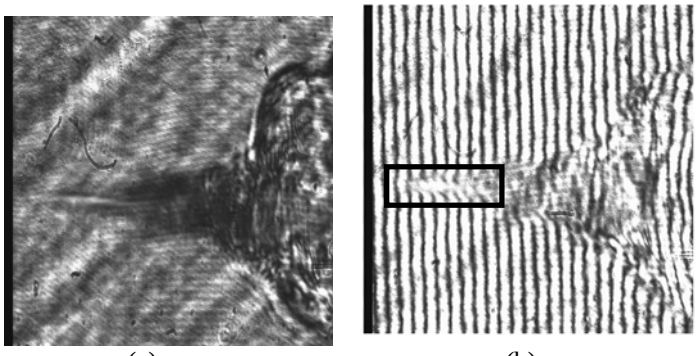

(a) (b)

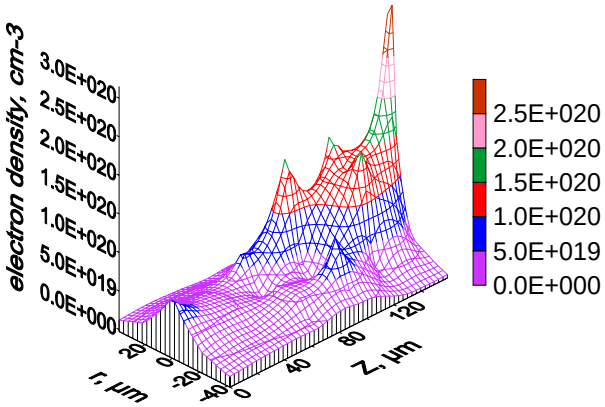

(c)

Figure 5. An absorption image (a), interferogram (b) and (c) electron density distribution for a marked area for a delay time t = 30 ps

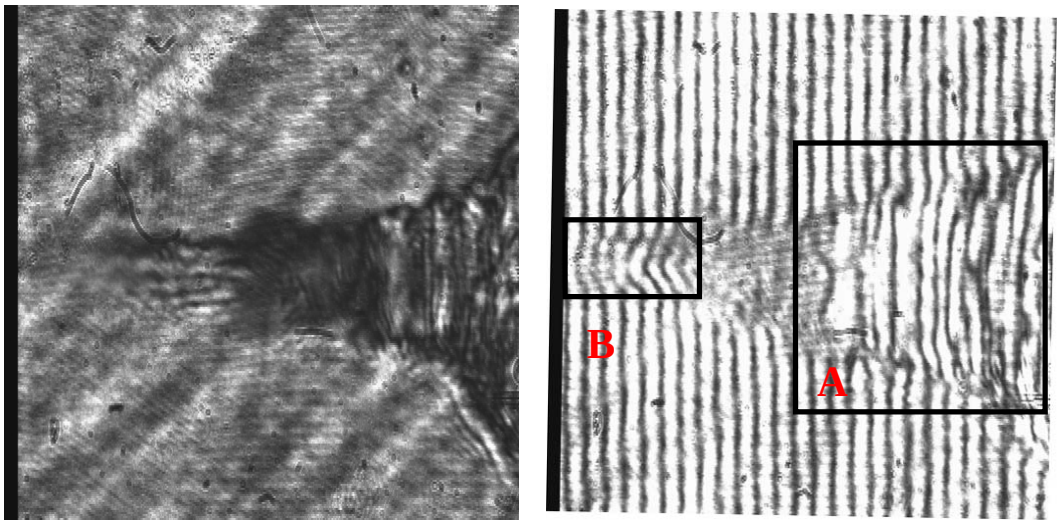

(a) (b)

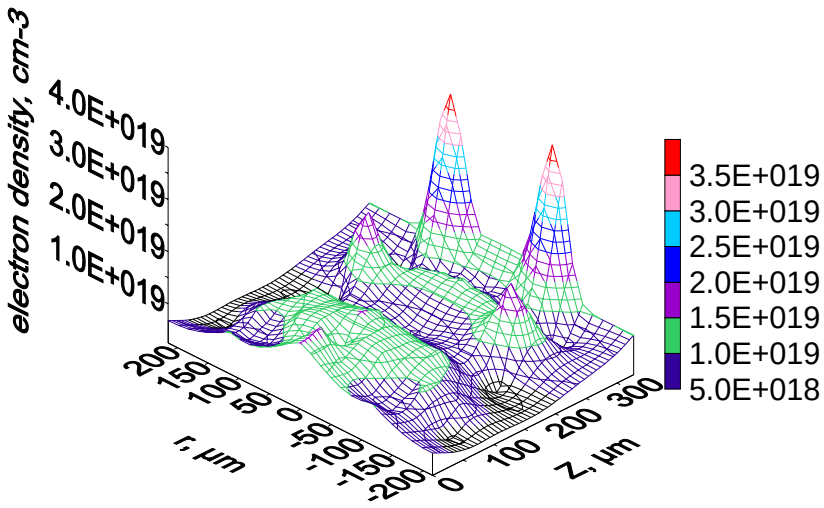

A (c)

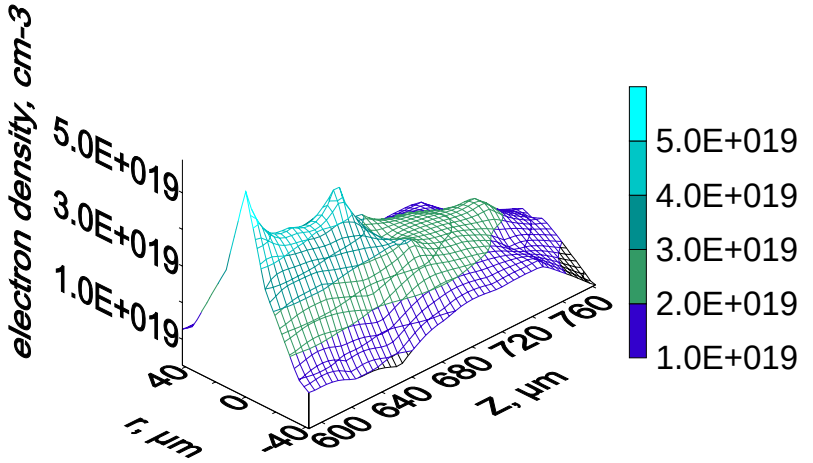

B (d)

Figure 6. An absorption image (a), interferogram (b) and electron density distribution for a marked areas A (c) and B(d) respectively.

5. 2. Megagauss Magnetic Fields Frozen in "Laser Bullets"

The large magnetic fields associated with resonant absorption in the plasma near the surface of critical density have been studied with the Faraday–rotation diagnostic system for the probe beam timing t = - 60ps, 0 ps, + 60 ps, +120 ps, +200 ps.

The Faraday rotation of the probing light appeared as early as – 60 ps, reached its maximum near + 60 ps, and then decreased again (it could be seen as late as + 200 ps). The results obtained for three probe-beam timing are shown in Fig.7a-f.

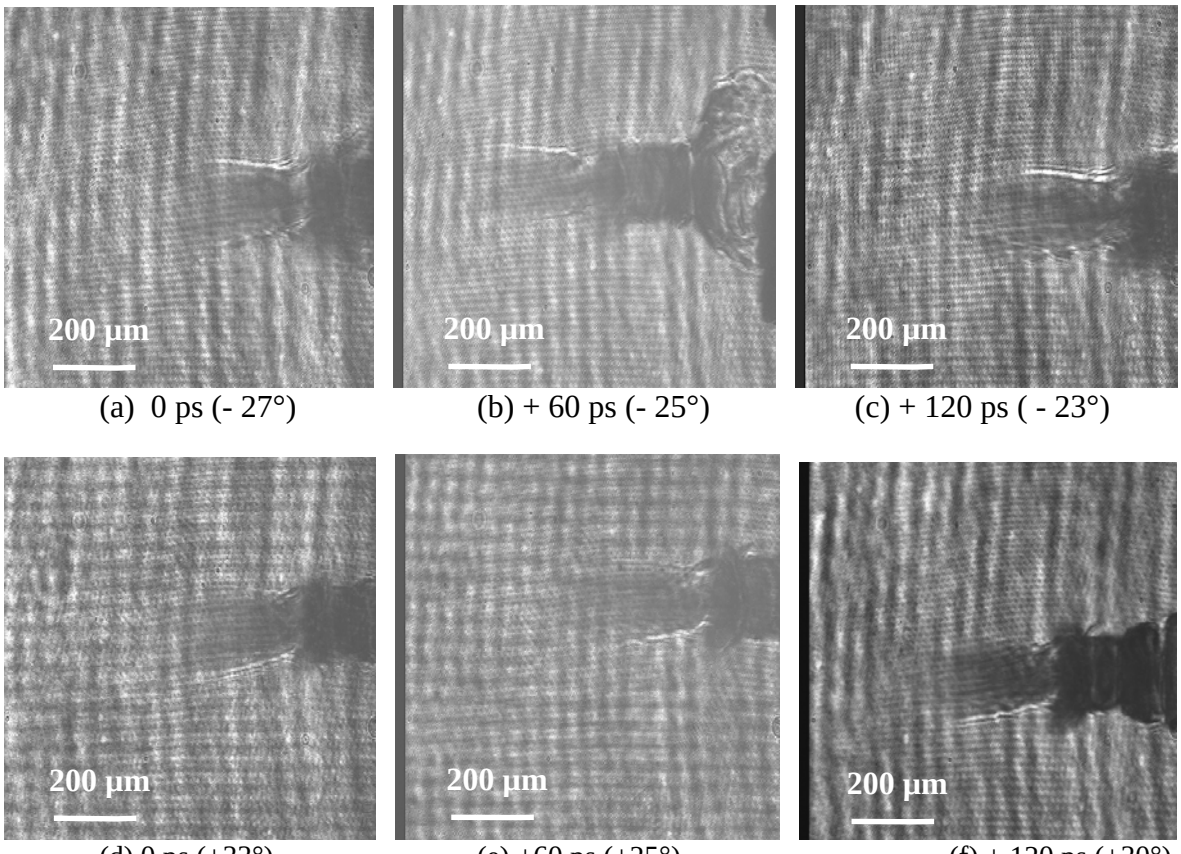

(a) 0 ps (- 27°) (b) + 60 ps (- 25°) (c) + 120 ps (- 23°)

(d) 0 ps (+33°) (e) +60 ps (+25°) (f) + 120 ps (+30°)

Fig. 7. Faraday – rotation photographs for probe-pulse timing t = 0, 60 ps and 120 ps. View into probing beam with main laser beam incident from the left. Analyzer orientation (with respect to the crossed position) is shown below each photograph and taken as positive when clockwise. The position of rotated light (bright stripes) reverses with reversal of analyzer orientation.

Each photograph shows the actual orientation of plasma target with plasma blocks near the surface of the shock wave front (with the main laser pulse incident from the left).

The orientation of each polarization analyzer (with respect to the crossed position) is indicated (in degrees) under the photograph. The well-localized thin bright stripes above and below the center of the plasma block are evident. The reversal of the analyzer orientation produces always a corresponding reversal in the position of the bright stripes. In opposite to the thermally generated magnetic fields the orientation of azimuthal magnetic field in plasma blocks is found to be consistent with the direction of the current flow driven by a ponderomotive force along the resonance absorption surface [24-25]. The magnetic field orientation and the current flow lines are shown schematically in Fig.8.

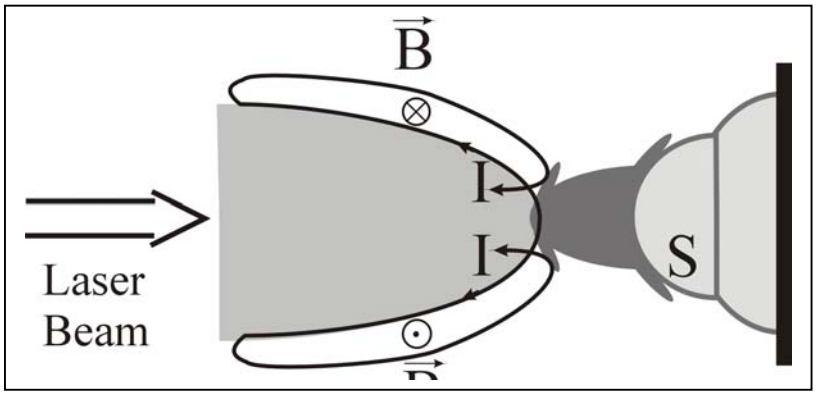

Fig.8. Schematic showing the target surface (T), the shock waves (S), the orientation of dc magnetic field (B) within the skin layer at the plasma-air interface , the lines of current flow giving rise to B.

The azimuthal direction remained unchanged throughout the observation interval (- 60 ps to + 200 ps) and the magnetic field lines were "frozen" in the moving massive plasma blocks (see Fig 9). Fig. 10 represents the ratio of the transmitted intensity in thin stripes to the background intensity versus the rotation angle of the polarizing sheet crossed position. Positive angles correspond to the rotation from the left to the right, when looking into the probing beam.

We estimate a typical rotation angle to be about 0.4 – 0.6 rad. By using electron density distribution determined by Abel inversion of interferograms (see Fig.11 a,b) and assuming that magnetic field varies inversely as the radial position in

plasma blocks, we can calculate the magnetic field magnitude required for this

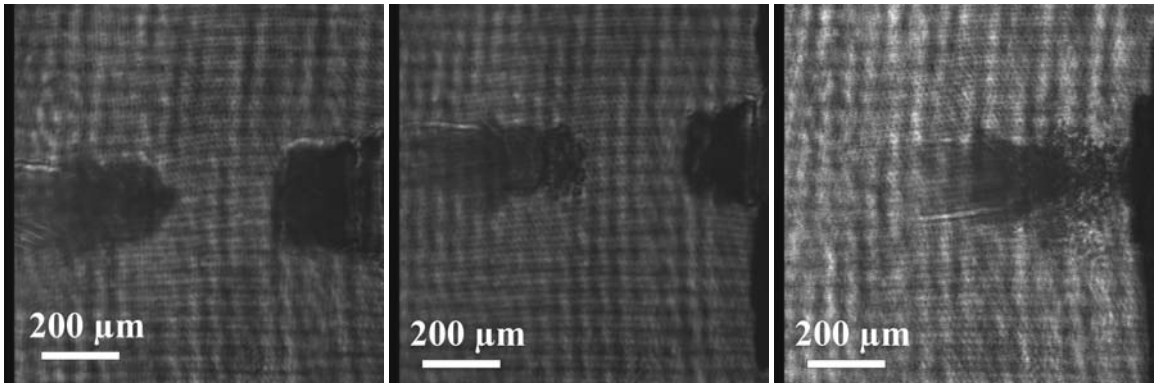

(a) + 60 ps (-25°) (b) + 60 ps (-42°) (c) +60 ps (+45°)

Fig. 9. Shadowgramms showing the "laser bullets" with "frozen " magnetic field.

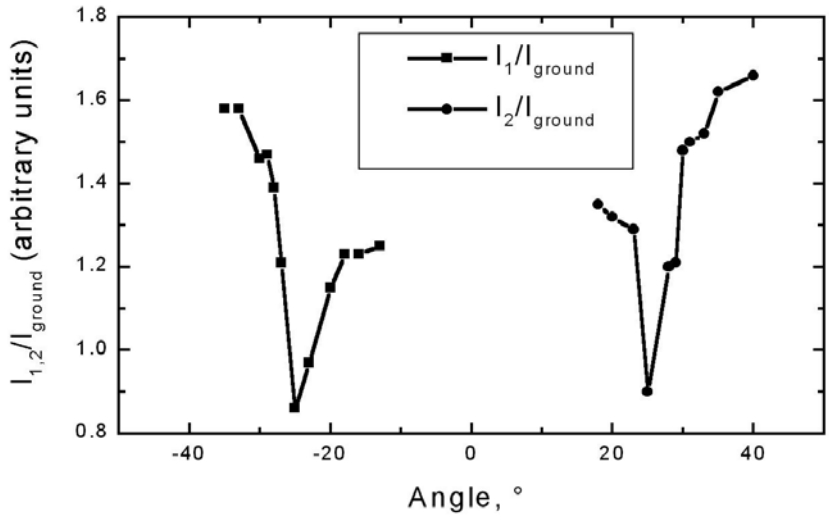

Fig. 10. Ratio of the transmitted intensity within the thin stripes to background intensity versus rotation angle of the analyzer for probe-pulse timing t = + 60 ps. I_1/I_{ground} – for lower and I_2/I_{ground} – for upper stripes in Fig.7

Faraday rotation angle. The calculated average values of magnetic field are of order 4-7 MGauss.

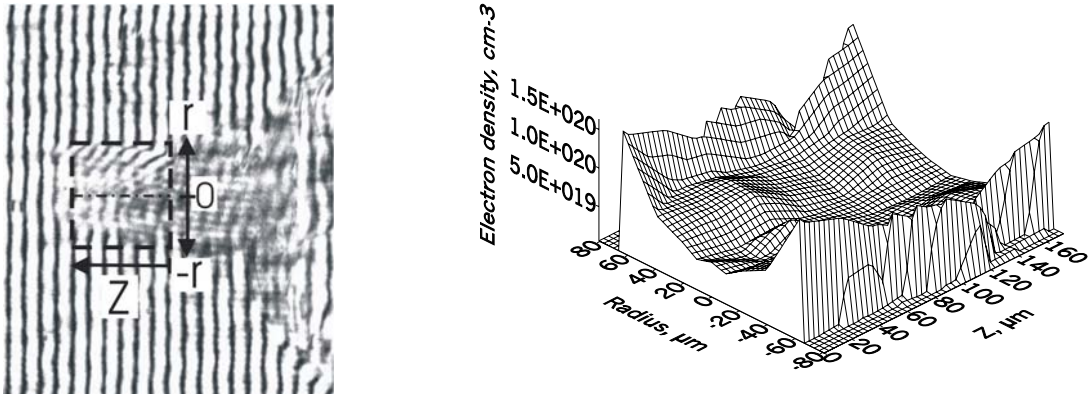

(a) (b)

Fig. 11. Interferogram (a) and electron density distribution (b) for probe-pulse timing t = + 60 ps.

Discussion of the results.

The physical mechanism for the generation of the observed high „dc“ magnetic field is quite simple. The magnetic field is generated by dc currents driven by the ponderomotive force of the laser pulse within the skin layer where resonance absorption of laser light occurs. It follows from high values of magnetic fields (4-7 MGauss) observed in our experiments, as well as from the structure of measured magnetic fields, which arise within the plasma layer and are oppositely directed to the thermo-electric fields. According with the plasma target geometry in our experiments (Fig.2b) the s-polarized incident beam is no strongly normal to the cutoff plasma surface and there is a component of the incident electric field (tangential component) along the resonance absorption surface which drives electrons in the skin layer. Theory predicts growth of dc magnetic fields due to resonance absorption approximately with the rate of 6 MG/psec [10], which is in reasonable agreement with the measured values (4 - 7 MG).

The physical mechanism for the blowing off the massive plasma blocks outwardly from the resonance absorption layer may originate from a magnetic ponderomotive force arising if a strong magnetic field is generated along the concave-convex surface of the resonance absorption layer. Lines of the current

flow which gives rise to the dc magnetic field are shown schematically in Figure 8. The force exerted by the magnetic field on the volume unit of a plasma block is given by $\mathbf{f} = N_e e [\mathbf{V_e} x \mathbf{H}]/c = [\mathbf{J} x \mathbf{H}]/c$.

The magnetic ponderomotive force is perpendicular to the plane [**JxH**]. It is directed inwards and has a blowing effect on the plasma block. The high-density moving plasma „bullets“ observed in our experiments are likely due to this effect. The „frozen“ magnetic fields in the plasma blocks keep them highly collimated.

In conclusion, we have demonstrated that the resonance absorption occurring near the shock wave front at the interaction of an intense laser pulse with a dense plasma is accompanied by generation of a strong „dc“ magnetic field and by blowing off massive plasma blocks due to magnetic ponderomotive force. Though the effect described above was investigated with a table-top device in laboratory, it is very similar to the generation of energetic outflows of gas from astrophysical objects, e.g. the young stellar objects [26], in which strong magnetic fields at large distance from the source have been observed. The outflows also are highly collimated and asymmetric [29], the radio emission from a number of outflows is non-thermal [28]. Similarly to the astrophysical jets, the crossing of current lines at r = 0 at the surface of resonance absorption observed in our experiments can lead to the crossing of magnetic field lines and to the explosive disruption of massive plasma blocks from the plasma body. The process is accompanied by a significant dissipation of power within the absorption layer. At the same time, the outflows of plasma convect the magnetic flux outwards.

References

[1] M. J. Herbst , J. A. Stamper , R. R. Whitlock, R. H. Lehmberg , B. H. Ripin , Phys. Rev. Lett., **46,** 328 (1981).

[2] C. Joshi , C. E. Clayton , K. Marsh et al., Opt. Comm., **70,** 44 (1989).

[3] N. G. Basov , A. A. Gamalii, A. E. Danilov et al., Pisma v ZETF, **38,** 60 (1983).

[4] N. E. Andreev , V. L. Arzimovich, V. T. Kasjanov, V. T. Tichonchuk, ZETF, **98,** 881 (1990).

[5] S.Jackel, B.Barry and M.Lubin, Phys. Rev. Lett., **37,** 95 (1976)

[6] R.A.M.Maddever, B.Luther-Davies and R.Dragila, Phys. Rev. **A41,** 2154 (1990)

[7] R.F.Turner, D.W.Phillion, E.M.Campbell and K.G.Estabrook Phys. Fluids, **26,** 579 (1983)

[8] H. Hora , *Plasmas at High Temperature and Density* (Springer, Heidelberg, 1991), p.204.

[9] R. N. Sudan, Phys. Rev. Lett., **70**, 3075 (1993)

[10] J.A. Stamper, K. Papadapoulos, R. N. Sudan, , S. O. Dean, E. A. McLean and J. Dawson, Phys. Rev.Lett., **26,** (1971), 1012

[11] A. Raven, O. Willi, P. T. Rumsby, Phys. Rev. Lett., **41,** (1978), 554

[12] J. A. Stamper, E: A: McLean; B. H. Ripin, Phys. Rev. Lett., **40**, (1978), 1177

[13] Y. Sakagani, H. Kawakani, S. Nugao, and C. Yamanaka, Phys. Rev. Lett., **42**, (1979), 839

[14] V. V. Korobkin, R. V. Serov, Pis‘ma v ZETF, **4**, (1966), 103

[15] G. A. Askar’yan, M. S. Rabinovich, A.D. Smirnova, V. B. Studenov, Pis‘ma v ZETF, **4**, (1967), 118

[16] J. A. Stamper, Laser Part. Beams, **9**, (1991), 841

[17] M. Borghesi, A. J. Mackinnon, R. Gaillard, O. Willi, A. Pukhov and J. Meyer-ter-Vehn, Phys. Rev. Lett., **80**, (1998), 5137

[18] M. Borghesi, A. J. MacKinnon, A. R. Gaillard, O. Willi, Phys. Rev. Lett., **81**, (1998), 112.

[19] A. J. Mackinnon, M. Borghesi, A. Iwase, and O. Willi, Phys. Rev. Lett., **80**, (1998), 5349

[20] S. V. Bulanov, F. Pergoraro, and A. M. Pukhov, Phys. Rev Lett., **74**, (1995), 710

[21] G. A. Askar'yan *et al* , Pisma v ZETF, (JETP Lett., **60**, (1994), 251)

[22] A. Pukhov and J. Meyer-ter-Vehn, Phys. Rev. Lett., **76**, (1996), 3975

[23] V. L. Ginzburg, Propagation of Electromagnetic Waves in Plasmas, Pergamon, N.Y. (1970)

[24] R. N. Sudan, Phys. Rev. Lett., **70**, (1993), 3075

[25] J. J. Thomson, C. E. Max, K. Estabrook, Phys. Rev. Lett., **35**, (1975), 663

[26] T. P. Ray, T. W. B. Muxlow, D. J. Axon, A. Brown, D. Corcoran, J. Dyson, R. Mundt, Nature, **385,** (1997), 415

[27] Bo Reipurth, John Bally, Robert A. Fesen, David Devine, Nature, **396**, (1998), 343

[28] S. Curiel, L. F. Rodriguez, J. Moran, M. Canto, J. Astrophys., **415**, (1993), 191